Journal of Biomechanics 147 (2023) 111440

Contents lists available at ScienceDirect

Journal of Biomechanics

journal homepage: www.elsevier.com/locate/jbiomech

Measuring compressive loads on a 'smart' lumbar interbody fusion cage: Proof of concept

Vivek A.S. Ramakrishna [a,b,c,*], Uphar Chamoli [b,d], Subhas C. Mukhopadhyay [c], Ashish D. Diwan [b,e], B. Gangadhara Prusty [a]

[a] School of Mechanical and Manufacturing Engineering, University of New South Wales, Sydney, Kensington, New South Wales, Australia
[b] Spine Labs, St. George & Sutherland Clinical School, University of New South Wales, Sydney, New South Wales, Australia
[c] School of Engineering, Faculty of Science and Engineering, Macquarie University, Sydney, New South Wales, Australia
[d] School of Biomedical Engineering, Faculty of Engineering and Information Technology, University of Technology Sydney, Ultimo, New South Wales, Australia
[e] Spine Service, Department of Orthopaedic Surgery St. George Hospital Campus, Kogarah, New South Wales, Australia

ARTICLE INFO

Keywords:
Smart implant
Interbody fusion
Interbody cage
Load sensing
Instrumented implant

ABSTRACT

There are several complications associated with lumbar interbody fusion surgery however, pseudarthrosis (non-union) presents a multifaceted challenge in the postoperative management of the patient. Rates of pseudarthrosis range from 3 to 20 % in patients with healthy bone and 20 to 30 % in patients with osteoporosis. The current methods in post-operative follow-up - radiographs and CT, have high false positive rates and poor agreement between them. The aim of this study was to develop and test a proof-of-concept load-sensing interbody cage that may be used to monitor fusion progression. Piezoresistive pressure sensors were calibrated and embedded within a polyether ether ketone (PEEK) interbody cage. Silicone and poly (methyl methacrylate) (PMMA) were inserted in the graft regions to simulate early and solid fusion. The load-sensing cage was subjected to distributed and eccentric compressive loads up to 900 N between synthetic lumbar vertebral bodies. Under maximum load, the anterior sensors recorded a 56–58 % reduction in pressure in the full fusion state compared to early fusion. Lateral regions measured a 36–37 % stress reduction while the central location reduced by 45 %. The two graft states were distinguishable by sensor-recorded pressure at lower loads. The sensors more effectively detected left and right eccentric loads compared to anterior and posterior. Further, the load-sensing cage was able to detect changes in endplate stiffness. The proof-of-concept 'smart' cage could detect differences in fusion state, endplate stiffness, and loading conditions in this *in vitro* experimental setup.

1. Introduction

Lumbar Interbody Fusion (LIF) surgery is a treatment option for low back pain that aims to immobilise and stabilise a degenerate, unstable spinal segment. An interbody cage is inserted between the vertebrae and its cavities are filled with osteoconductive material that promotes bone growth through the implant until the two vertebrae are fused. While there are a number of complications associated with LIF surgery, such as implant subsidence, pseudarthrosis presents a multifaceted challenge in the postoperative management of the patient.

Pseudarthrosis is the incomplete bony union between the adjoining vertebrae following LIF surgery, characterised by persistent pain and associated with several other complications (Meng et al., 2021). The time taken to reach full bone fusion may vary from 6 to 12 months, however rates of pseudarthrosis at least one year after LIF surgery range from 3 to 20 % in patients with healthy bone (Fogel et al., 2008; Manzur et al., 2019; Meng et al., 2021; Nakashima et al., 2011). Non-union is a higher risk factor for patients with poor bone quality, occurring in 20–30 % of patients with osteoporosis (Chun et al., 2015; Vaidya et al., 2008; Wu et al., 2012). Numerous other factors, such as bone graft biologics (Hsu et al., 2012), implant material (Meng et al., 2021), and lifestyle choices (Carpenter et al., 1996; Emami et al., 2018; Hadley and Reddy, 1997; Sawin et al., 2001) are associated with pseudarthrosis, emphasising the importance of effectively monitoring the ossification process in the postoperative phase.

There is, however, a considerable degree of ambiguity in the

* Corresponding author at: 208, Level 2, J17 School of Mechanical and Manufacturing Engineering The University of New South Wales, Kensington, NSW 2052, Australia.
E-mail address: v.ramakrishna@student.unsw.edu.au (V.A.S. Ramakrishna).

https://doi.org/10.1016/j.jbiomech.2023.111440
Accepted 6 January 2023
Available online 9 January 2023

assessment of the bony fusion mass following a spinal fusion surgery that makes the diagnosis of pseudarthrosis challenging (Chun et al., 2015; Umali et al., 2019). Surgeons currently rely on different imaging measures to assess bone maturity in the fusion mass, including the absence of radiolucent gaps, increasing opacification, indications of trabecular bone bridging, and negligible motion on flexion–extension radiographs (Hayeri and Tehranzadeh, 2009; Oshina et al., 2018; Ramakrishna et al., 2020; Umali et al., 2019). Furthermore, there is no clear standard for the determination of radiologically assessed 'negligible' motion (Chun et al., 2015). Plain radiographs have been shown to be ineffective at detecting pseudarthrosis (Klineberg et al., 2016) and radiologically determined solid fusion may not correlate with biomechanically solid fusion (Ramakrishna et al., 2020). The two standards for assessing fusion - plain radiographs and fine-cut CT, were previously classified as fair to moderate for interobserver and intraobserver reliability (Carreon et al., 2007; Carreon et al., 2008). Agreement on fusion grade between the two imaging modalities was only 46–59 % (Carreon et al., 2007). A high false-positive rate has also been reported using CT to determine solid fusion of the bridging mass (Carreon et al., 2008). There is an evident need to investigate more sensitive and specific approaches to monitoring bony growth in the fusion mass after LIF surgery.

The evolution of instrumented sensor-enabled implants, or 'smart' implants, continues to re-shape the course of musculoskeletal care. Sensors are being designed with the specific purpose of monitoring bone healing in fracture fixation plates (Borchani et al., 2016). In several studies, sensors embedded in spinal fusion rods have been used to monitor loads after fusion surgery without monitoring fusion progression (Lin et al., 2007; Rohlmann et al., 1994, 1999; Rohlmann et al., 1995). More recently, Windolf et al. demonstrated a sensor-recorded reduction in load on the fusion rods as the fusion mass ossified in the facet joint gap of a single sheep (Windolf et al., 2022). In an instrumented interbody cage, Ledet et al. quantified loads on the implant in two baboons (Ledet et al., 2000; Ledet et al., 2005). While the six-week measurement period was insufficient to monitor bony fusion, it demonstrates that obtaining direct measurement from embedded sensors in an interbody cage is feasible (Demetropoulos et al., 2009; Ledet et al., 2000; Ledet et al., 2005).

Given the shift towards 'smart' implants in orthopaedics, the complications of pseudarthrosis, and the limitations of its diagnosis, it is pertinent to investigate the feasibility of sensors in interbody cages for monitoring the progression of fusion after LIF surgery. The aim of this study was to develop a proof-of-concept load-sensing interbody cage for detecting bone graft stiffness changes while subjected to distributed loads, eccentric loads, and endplate stiffness changes in an *in vitro* experimental setup.

2. Material and methods

2.1. Sensors and Printed Circuit board design

Amphenol P122 High Silicon Pressure Sensor Dies (Novasensor) were integrated with the interbody cage due to its piezoresistive operating principle, embeddable size (2.5 × 2.5 × 2.0 mm), regular shape, and suitable pressure limit. Many other sensor options did not simultaneously meet the criteria for size or shape, such that they may be implantable, and withstand the required loads. Data was extracted from sensors embedded at 5 locations in the interbody cage as shown in Fig. 1.

Two Printed Circuit Boards (PCBs) were designed to control data transfer from the sensors and allow them to be embedded into the interbody cage. PCB-A was a small PCB onto which the sensors were bonded using flip-chip bonding. PCB-B largely followed the geometry of the interbody cage with an extruded edge that held connections for data transfer and processing. PCB-A was hand-soldered to PCB-B at the required locations.

2.2. Interbody cage design and manufacturing

A modified Extreme Lateral Interbody Fusion (XLIF) cage was designed. XLIF cages generally have a larger footprint compared to other surgical approaches, which provided the required space for sensors and PCBs.

The XLIF cage (22.0 × 50.0 × 14.5 mm, 0° lordosis) was manufactured using CNC milling from polyether ether ketone (PEEK) material supplied by Dotmar Engineering Plastics (North Rocks, NSW 2151, Australia). Cavities were designed for the graft (17.3 × 11.0 mm) in addition to cuts through the vertical faces of the cage that allow for bone growth in commercially available XLIF fusion implants (Fig. 2).

2.3. Sensor calibration

Sensor calibration was performed by applying load directly to each sensor individually up to 1.5x its operating pressure (overpressure limit

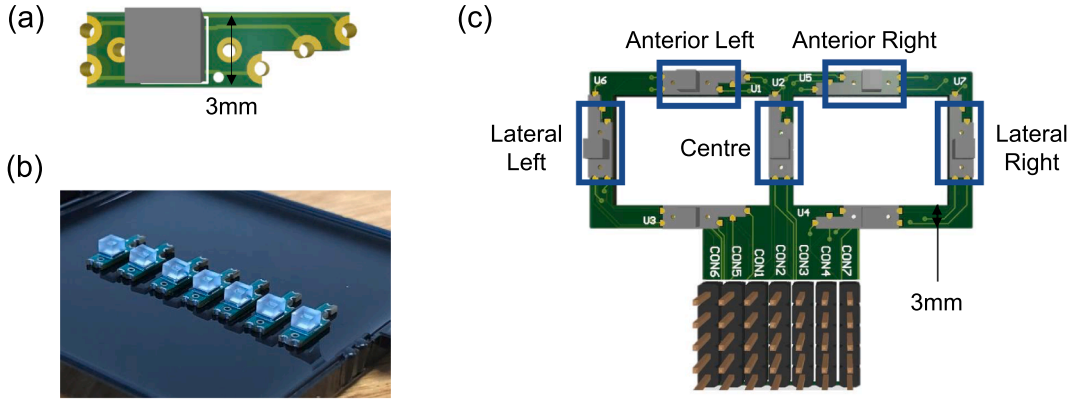

Fig. 1. Design of PCB-A (a) with maximum dimensions of 10.50 mm × 3.00 mm, flip-chip bonded die (b), and PCB-B (c) with maximum dimensions of 48.90 mm × 20.00 mm for the region embedded within the implant. The thickness of PCB-A was 0.41 mm; the thickness of PCB-B was 1.16 mm. The pressure sensing dies were bonded to PCB-A using flip-chip bonding. Gold bumps were bonded to the PCB attachment pads using the TPT HB100 Wire Bonder and 25 μm gold wires at 150 °C (100mW, 200 ms, 250mN). A Finetech Fineplacer Lambda Die Bonder was used to apply thermocompression bonding, with a force of 4 N for 60 s at 320 °C, to attach the pressure sensor die to PCB-A. EpoTek 301–2 epoxy was applied as an underfill between the die and PCB-A, and desiccated in a vacuum for 20 min before curing at 80 °C for 3 h.The sensors were soldered to 5 locations (c); Lateral Left (Lat Left), Anterior Left (Ant Left), Centre, Anterior Right (Ant Right), and Lateral Right (Lat Right).

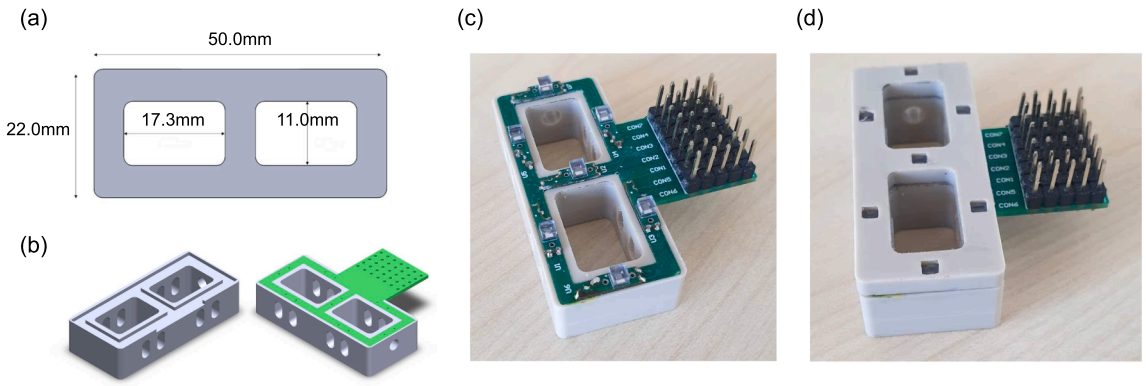

Fig. 2. Interbody cage design and dimensions (a-b). Slots were machined in the cage to house and enclose the sensor-mounted PCB (c-d). 0.5 mm of room-temperature vulcanising silicone was applied on the sensor surfaces and levelled to the cage surface to protect the sensors from damage during loading.

= 2x), using an ESM-Mark10, and recording the analogue to digital conversion (ADC) output. The ADC output was calibrated against the known applied pressure. Calibration curves were produced for each sensor (see Supplementary Information 1).

2.4. Graft materials

Two unique states of bone fusion were simulated by different graft materials. Silicone represented the early stage of spinal fusion. Depending on the type of graft used, the histological characterisation of this early stage may be different. The bone formation represented by silicone may be inclusive of endochondral, fibro-cartilaginous, or membranous histological stages, or a combination of these stages, which is mechanically non-solid (Ramakrishna et al., 2022). Poly(methyl methacrylate) (PMMA) was used to represent late-stage ossification of the bony fusion mass (solid fusion), however may also be representative of stiffer bone grafts, such as allografts.

2.5. Loading conditions

The sensor-embedded cage was placed between two blocks of synthetic bone (Sawbones) of similar dimensions to a lumbar vertebral body (50 × 35 × 30 mm), consisting of a 2 mm layer of cortical bone and 28 mm of cancellous bone. All loads were applied with an Instron 3369 (1kN load cell) to 900 N at 0.6 mm/min for 3 trials. Sensor output was recorded during the load tests to measure pressure in response to changes in graft stiffness with different contacting bone stiffnesses and load types.

2.5.1. Distributed load

A 3 mm thick aluminium plate was placed on the superior surface of the synthetic vertebral body to ensure even distribution of the load. The distributed load was applied with the cancellous bone contacting the cage surface (cancellous contact). The load test was completed with silicone and PMMA graft materials.

The vertebral body was inverted such that the cortical bone was contacting the interbody cage surface (cortical contact) and the distributed load tests were repeated with both silicone and PMMA grafts.

2.5.2. Eccentric load

Eccentric loads were applied with cancellous contact only. Loads were applied individually at 4 different locations around the cage centre (without the aluminium plate) as indicated in Figs. 3 and 4.

2.6. Finite element analysis

A 3D finite element (FE) model was developed in Strand7 FE analysis software (vers. 2.4.6, Strand7 Pty. ltd.) as a validation tool for the sensor

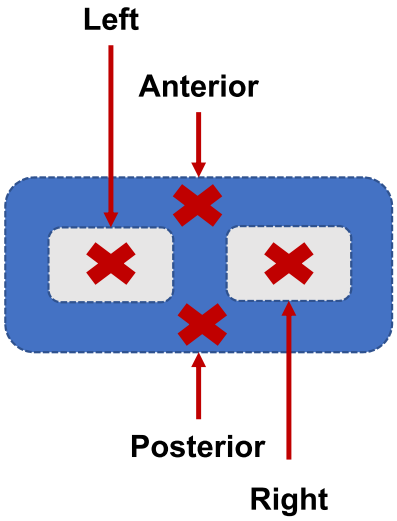

Fig. 3. Top view of the load-sensing cage showing the four points of eccentric load application, each applied separately.

outputs and to determine an indicative predicted shift in expected pressure as a result of changing the graft and contact material. The model was developed to replicate the experimental setup (material properties presented in Table 1). A symmetrically-halved model geometry was built in Strand7, including the top and bottom synthetic cancellous and cortical bone, reducing the computational time and allowing for a finer mesh. As such, the cross-sectional plane was constrained by a symmetric boundary. The nodes on the bottom surface were constrained in all translational and rotational degrees of freedom. The model was loaded in compression from the top surface with an evenly distributed load equivalent to 450 N.

3. Results

Three trials were conducted for each experimental loading scenario with averages reported in the results below.

3.1. Distributed load

Sensor-recorded measurements showed a reduction in pressure at all locations in the solid fusion state compared to early fusion with cancellous contact (Fig. 5). Under the maximum 900 N load, there was a 58 % and 56 % reduction in pressure in the anterior left and right sensors respectively. Pressure on the centre sensor reduced by 45 %, while lateral left and right sensors reduced by 36 % and 37 % respectively.

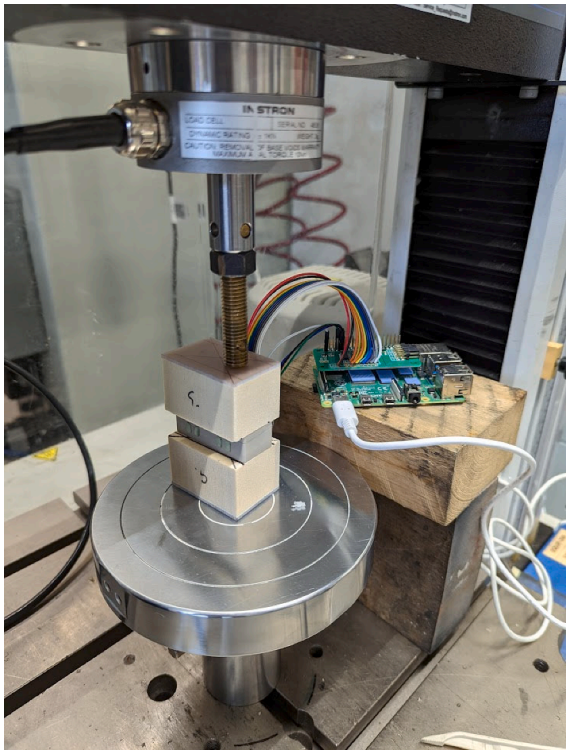

Fig. 4. Loading setup of the sensor-enabled cage for left eccentric load in an Instron 3369 Universal Testing Machine.

Table 1
Material properties used in developing the finite element model for validation. The model consisted of 501,358 bricks and 525,522 nodes, mostly consisting of 0.5 × 0.5 × 0.5 mm brick elements where straight edges were achievable in the model geometry.

Material	Material Model	Properties E: Elastic Modulus (MPa) G: Shear Modulus (MPa) κ: Bulk Modulus (MPa) ν: Poisson's Ratio ε: Strain (%)	Source
PEEK	Isotropic	$E = 3750$ $\nu = 0.38$	Manufacturer supplied
Sawbones Cancellous	Isotropic	$E_{Tension} = 284$ $E_{Compression} = 210$	Manufacturer supplied
Sawbones Cortical	Isotropic	$E_{Tension} = 16000$ $E_{Compression} = 17000$	Manufacturer supplied
FR4 PCB	Orthotropic	$E_{xx} = 22000$ $E_{yy} = 22000$ $E_{zz} = 9800$ $G_{xy} = 3500$ $G_{yz} = 3500$ $G_{xz} = 2500$ $\nu_{xx} = 0.28$ $\nu_{yy} = 0.28$ $\nu_{zz} = 0.11$	(Wang et al., 2006)
Silicone	NeoHookean	$C = 0.207$ $\kappa = 20.7$ MPa	Manufacturer supplied
PMMA	Isotropic	$E = 2700$ $\nu = 0.42$	(Orr et al., 2003)
Silicon Die	Isotropic	$E = 130000$ $\nu = 0.28$	(Hopcroft et al., 2010)

Similarly with cortical contact, pressure measured in the interbody cage was lower with solid fusion compared to early fusion under a 900 N distributed load (Fig. 6). The anterior left and right pressures reduced by

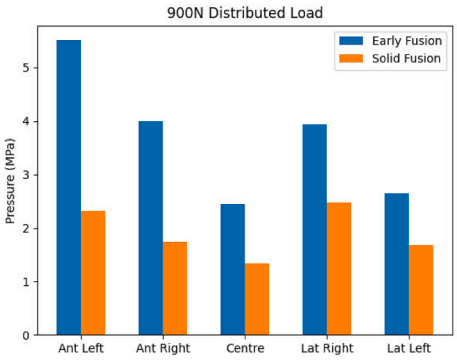

Fig. 5. Pressure measured at each sensor location with cancellous contact under 900 N distributed load.

56 % and 60 % respectively, however the centre sensor recorded a 71 % reduction in stress with solid fusion. Pressure recorded at the lateral locations reduced by 63 % (right) and 51 % (left). Lateral and centre sensors demonstrated a larger reduction in stress with graft stiffness when the contacting bone was stiffer.

At the anterior left and right locations, pressure was higher with the stiffer cortical bone compared to cancellous (Early Fusion: Ant Left = 25 %, Ant Right = 21 %; Solid Fusion: Ant Left = 32 %, Ant Right = 13 %), however, in the lateral regions the opposite trend was observed (Early Fusion: Lat Left = -10 %, Lat Right = -6%; Solid Fusion: Lat Left = -31 %, Lat Right = -44 %) (Fig. 6). No considerable difference was measured at the centre sensor with the silicone graft. At solid fusion, however, pressure was 46 % lower at the centre location with cortical contacting bone.

There were no clear trends in pressure differential between early fusion and solid fusion as the load increased up to 900 N (Fig. 7). For each sensor, the measured pressure difference tended to be consistent and distinguishable between the two graft states regardless of the stiffness of contacting bone. In the early fusion state, the highest absolute pressure was measured at the anterior left sensor (Cancellous = 5.51 MPa; Cortical = 6.91 MPa). With solid graft, the lateral right sensor recorded the highest pressure with cancellous contact (2.48 MPa); the anterior left sensor with cortical contact (3.06 MPa). The lowest pressures were measured at the centre location in the solid fusion state (Cancellous = 1.33 MPa; Cortical = 0.72 MPa). At early fusion, the centre pressure was lowest with cancellous contact (2.45 MPa), while the lateral left the was lowest with cortical contact (2.39 MPa).

3.2. Simulation comparison

Pressure measurements were extracted from the FE models as average and maximum compressive stresses in each sensor region (Fig. 8). Experimentally obtained measurements were, for most cases, within the range of the average and maximum values obtained from the FE analysis. The anterior left pressure was higher than the maximum obtained from simulation in the early fusion state (Cancellous = 4 %; Cortical = 14 %). The lateral right sensor measured a 2 % higher stress than the simulation value with silicone graft and cancellous contact. In the solid fusion state with cortical contact, the centre sensor measured 19 % lower stress than the average obtained from simulation.

3.3. Eccentric loads

The percentage change in measured pressure between the eccentric load and distributed load is shown in Fig. 9. Anterior loading resulted in an increase in stress in the anterior sensors and reduced stress in remaining sensors, with the exception of the lateral right sensor in the early fusion state. Similarly, posterior loading reduced stress in the anterior locations. Left eccentric loading increased stress in the lateral

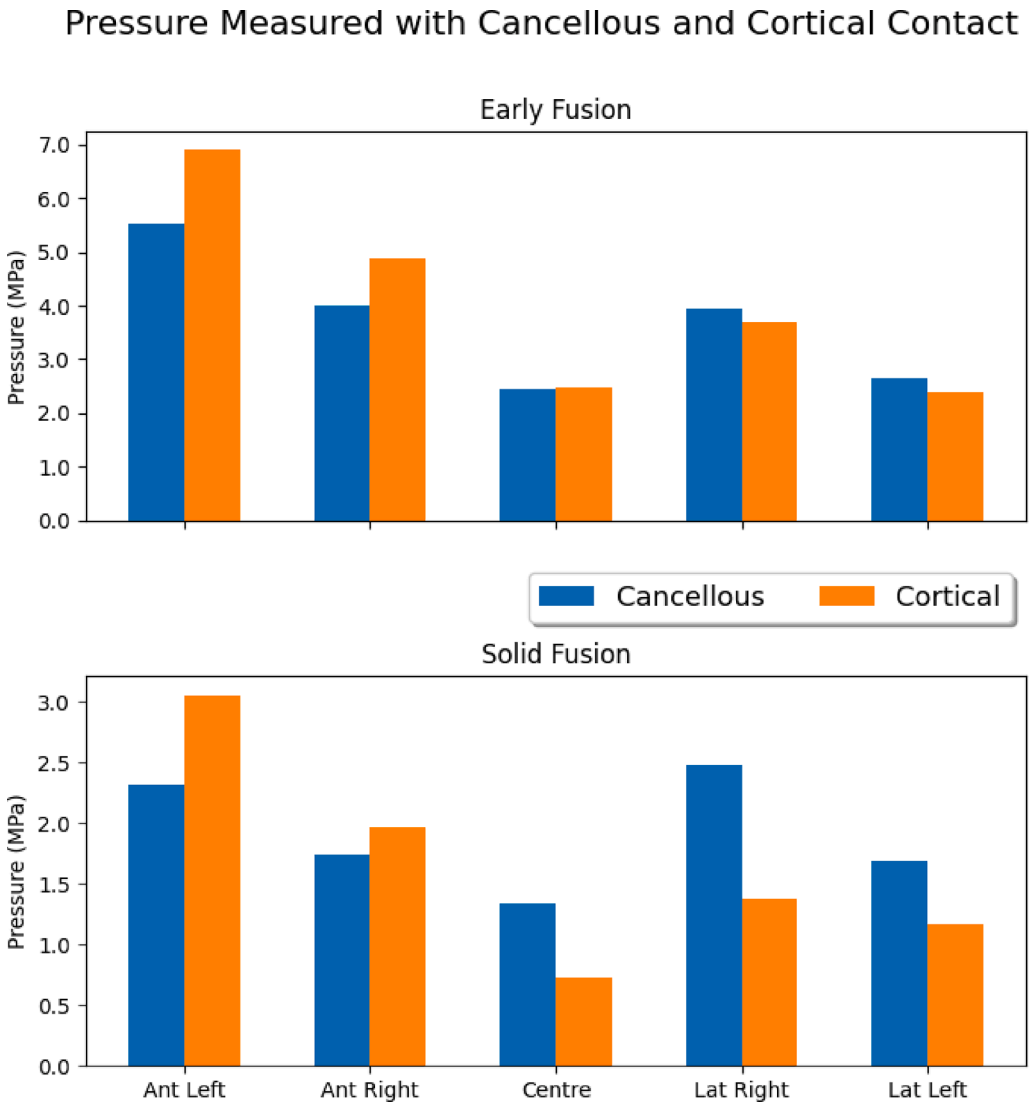

Fig. 6. Pressure measured at each sensor location under 900 N distributed load comparing cancellous and cortical contact.

left and anterior left locations while stress on all other sensors reduced. A similar pattern was found under right eccentric loading, with lateral right and anterior right stresses increasing and all others demonstrating reduced stress. The magnitude of change between each eccentric load and the distributed load was higher with solid fusion compared to early fusion. Absolute pressure values are presented in Supplementary Information 2: Table S1.

4. Discussion

The aim of this study was to develop and test a proof-of-concept load-sensing interbody cage with the aim of determining whether sensors embedded within the PEEK implant can detect stiffness changes in the graft region evaluated with a distributed load, eccentric loads, and with different contacting bone stiffnesses. Sensor-enabled interbody cages have been used to assess loads *in vivo* (animal) and *in vitro* (cadaver), however the findings were not associated with fusion progression or endplate health (Demetropoulos et al., 2009; Ledet et al., 2000; Ledet et al., 2005).

Under a distributed load, the load-sensing cage demonstrated good differentiation between the early fusion and solid fusion states, where the solid graft off-loaded the interbody cage. With cancellous contact, the reduction in sensor-recorded stress ranged from 36 to 58 % depending on sensor location. The reduction in stress at the anterior of the cage was larger than the lateral region; a pattern that was consistent with the simulation results. The FE analysis, however, showed the largest off-loading of the cage in the central region. Borchani et al. demonstrated the feasibility of using piezo floating gate sensors to monitor bone healing in a femoral fracture fixation plate, differentiating between different states of bone healing (Borchani et al., 2016). Similarly, the results of this study demonstrate the measurable difference in fusion implant stress at the two endpoints of bone healing: early bone formation and solid fusion. Expanding the scope of this study may allow for the construction of bone-healing curves that account for more bone formation conditions and growth into the endplates.

Sensors in the interbody cage were able to detect regional pressure variation resulting from changes to stiffness of the contacting bone. Compared to cancellous contact, the anterior of the cage experienced more stress with cortical contact while the lateral regions were off-loaded. These patterns were consistent in both early and solid fusion states. There is a load-pattern shift that occurs away from the lateral regions and towards the anterior of the cage with stiffer contacting bone. The long axis of the cage spans the lateral vertebral width, whereas the short axis of the cage does not span the anterior-posterior dimension of the vertebrae. As such, micro-deformation of the cancellous bone contacting the implant is more likely to occur at the anterior of the cage.

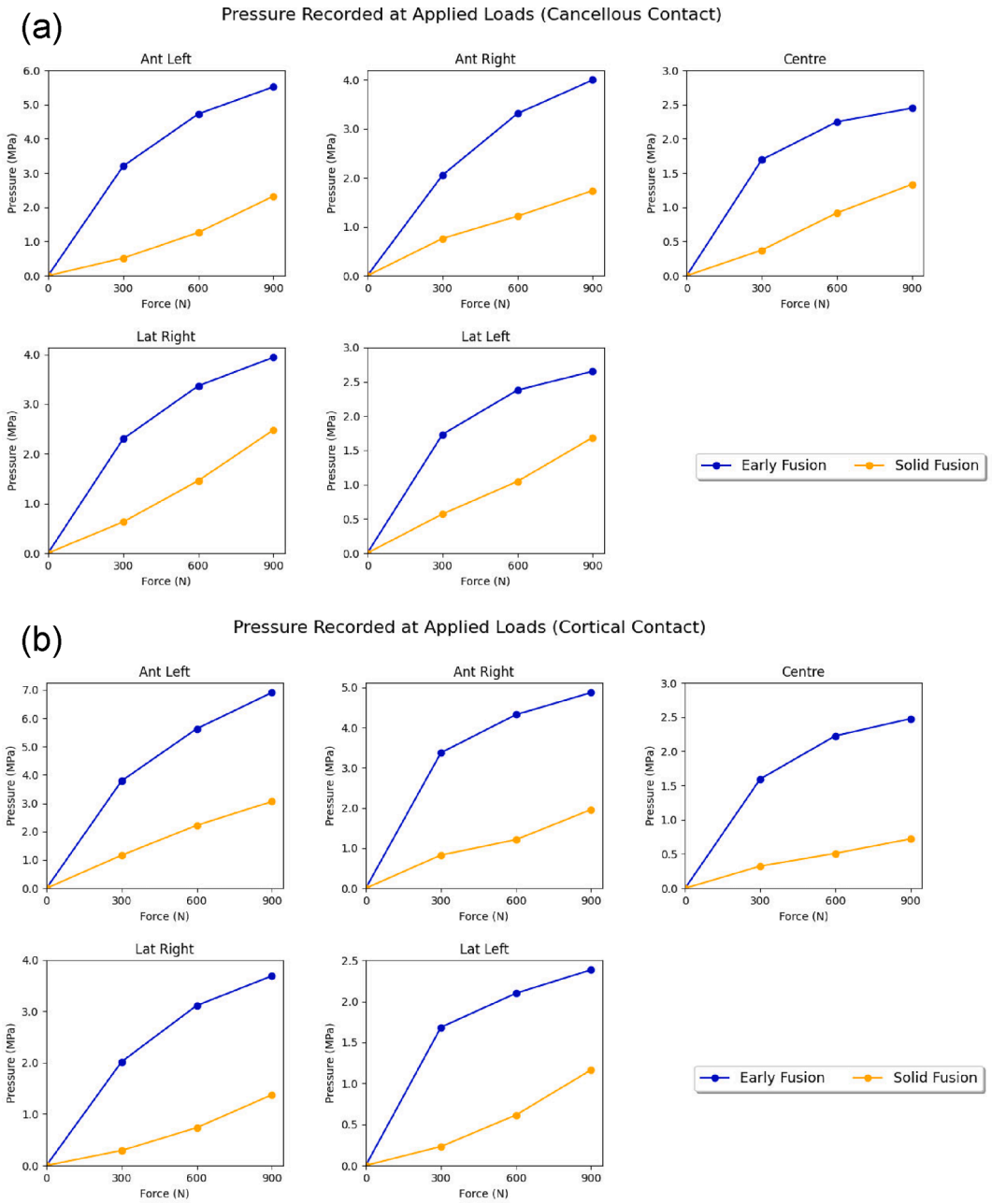

Fig. 7. Pressure measured at distributed loads from 0 to 900 N with cancellous (a) and cortical (b) contact in both fusion states.

Larger deformation of the bone would likely cause less load to be transferred to the anterior of the implant. With the cortical bone deforming less, a load-shift occurs towards the anterior of the cage and away from the lateral and central regions with cortical contact. These load-pattern changes have been found in the simulation results, demonstrating that the sensors are detecting the trend of an expected load-shift (Supplementary Information 2: Table S2). The magnitude of change measured by the sensors is, however, larger than expected in most regions.

Cancellous and cortical contact have been used to emulate different endplate conditions. Given pseudarthrosis rates vary between osteoporotic and healthy patients, and the incidence of subsidence, measurements from the interbody cage that differentiate between endplate stiffness states may be clinically relevant. Sensor-enabled fusion rods have been studied extensively, with previous research unable to use the devices to assess fusion progression (Lin et al., 2007; Rohlmann et al., 1994, 1999; Rohlmann et al., 1995; Szivek et al., 2005). Szivek et al. were not able to detect reduced loads on the fusion rod as fusion progressed, however successfully measured this change from sensors placed directly on the lamina (Szivek et al., 2005). A recently published animal study by Windolf et al. demonstrated 'smart' fusion rods can monitor fusion mass ossification in the region between the facet joints (Windolf et al., 2022). These results suggest achieving accurate monitoring of fusion progression may require sensors to be embedded proximate to the fusion mass. Further, sensor-embedded fusion rods are unable to detect mechanical changes in the endplates.

Sensors at the anterior of the cage were loaded more with anterior eccentric loading and less with posterior loading compared to the distributed load results. However, results from the lateral sensors under anterior and posterior loads showed mixed patterns. Left and right eccentric loads resulted in the expected loading pattern, increasing stress on the proximate sensors and reducing stress on the distant sensors compared to distributed loading. The magnitude of the pressure change at each location between eccentric and distributed load cases was

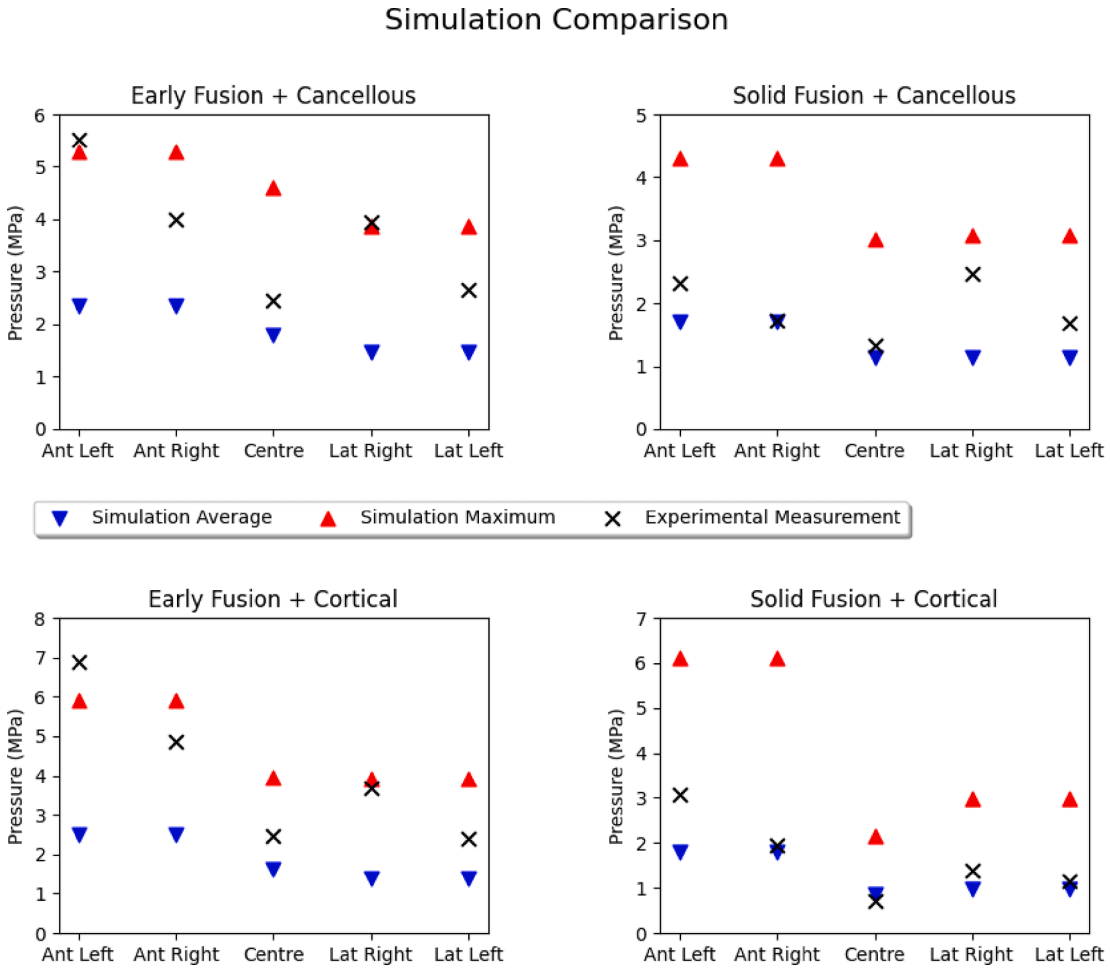

Fig. 8. Comparison between simulation and experimental data for the distributed load case. The sensor regions in the simulation occupy a volume containing multiple brick elements. As such, the average and maximum values in the sensor regions are presented here.

considerably higher with solid fusion compared to early fusion. With early fusion, the pressure difference between distributed and eccentric loads is smaller, as the cage bears a higher share of the load compared to the graft. The solid graft, however, offloads the cage. As such, the cage experiences a more substantial stress redistribution under eccentric loading at the point of solid fusion. At most locations, the graft states remained distinguishable by pressure measurement (Supplementary Information 2: Table S3). Generally, sensors distant from the eccentric load showed the greatest pressure differential between the two graft states. The results suggest that the current sensor layout is able to distinguish between the graft states and different eccentric loads, however alterations to this sensor layout may not be able to establish the same.

Through a proof-of-concept design, this study demonstrates the load-sensing interbody cage is a feasible technology to assess progressing bony union and endplate stiffness under different loading conditions. The research conducted has prioritised obtaining experimental data from the 'smart' implant, laying the foundation for further development, optimisation, and sensor reduction for improved implantability *in vivo*. The literature has established the wide-ranging utility of 'smart' interbody cages and fusion rods (Ledet et al., 2012; Ledet et al., 2005; Lin et al., 2007; Rohlmann et al., 1994, 1999; Rohlmann et al., 1995; Szivek et al., 2005; Windolf et al., 2022), while the research presented in this study specifically shows the response of the 'smart' cage to different graft stiffnesses, endplate stiffnesses, and loading conditions *in vitro* using a spatial sensing distribution. These measures further the clinical utility of a 'smart' fusion cage, with applications in monitoring fusion progression, endplate health, and subsidence risk. With further development, load-sensing interbody cages may replace periodic radiological follow-up (exposing patients to ionising radiation with limited diagnostic reliability), and ultimately reduce complication rates (Ramakrishna et al., 2020).

Some inconsistencies were noted in the experimental results. Under a distributed load, sensor measurements varied between locations that were symmetrically aligned on the cage. Further, while the experimental measurements generally followed the trends obtained from FE analysis, there were discrepancies in the magnitude of those trends. The design and manufacturing of the load-sensing cage was complex, introducing several points (sensor to PCB-A, PCB-A to PCB-B, cage to sensing-board) at which loading inconsistencies could be introduced, accounting for both intra-cage pressure variation and discrepancies between experimental and simulation data. The complex material interaction between the different components of the device presented an additional modelling challenge that may have introduced inaccuracies.

With the simulation modelling the volume of the sensor, it is unclear whether the true comparison between the FE model and sensor measurement is the average of stress in the sensor region, the maximum stress, or stress at any other defined point within the sensor region. While FE analysis is a useful comparison, it is not the most suitable validation method. The designed system lacks sensing validation due to an absence of available comparable sensors. Sensors of different size and shape would require changes to the cage geometry to encapsulate them, reducing confidence in their comparative value. While the results of this study sufficiently assess the ability of this proof-of-concept design to

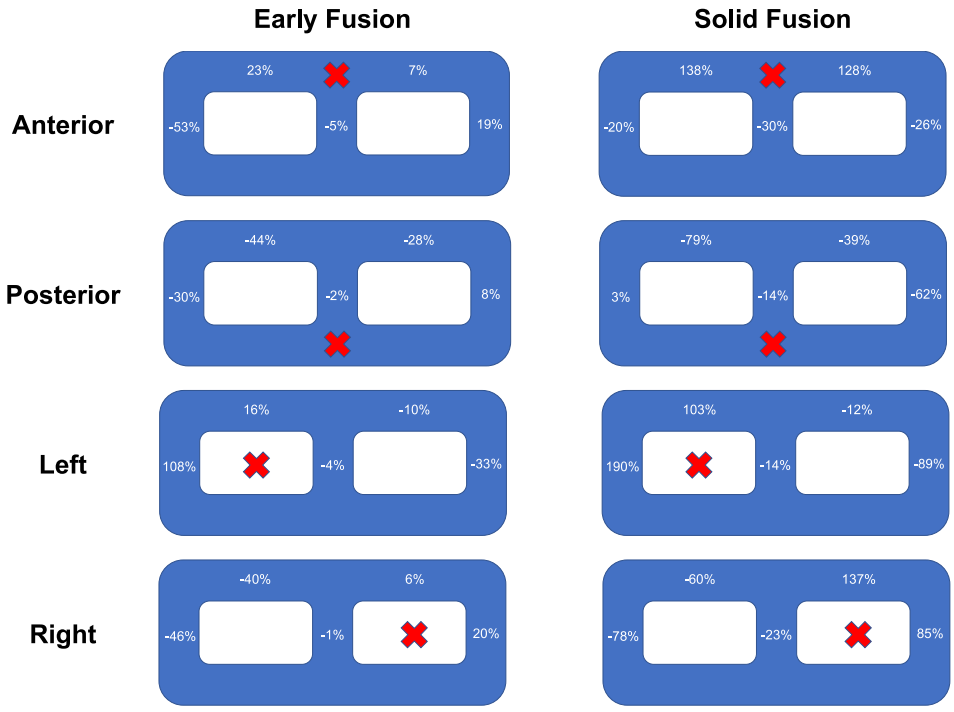

Fig. 9. Percentage difference in pressure recorded at each sensor location with respect to the distributed load case, where X depicts the location of the eccentric load applied. Anterior direction at the top of the page.

monitor fusion and endplate changes, a suitable validation method should be sought in future works.

Variation in pressure measurements over the three trials may indicate sensor degradation or damage. Further, sensor drift is likely to occur with consistent static loading over a long period of time *in vivo*. The conducted experiments are not able to evaluate the impact of sensor drift. Future research should aim to identify durable sensing modalities and perform long-term drift studies to identify encapsulation and compensation methods to address this limitation.

At this proof-of-concept stage, the loading scenarios investigated were basic and endplates were limited to cancellous and cortical material due to the absence of better synthetic equivalents. While the XLIF cage design was suitable for the study conducted, this is a notable limitation given the prevalence of smaller interbody cages and expandable cages in clinical practice.

5. Conclusion

The proof-of-concept load-sensing interbody cage can detect differences in fusion state, endplate stiffness, and loading conditions in this *in vitro* experimental setup. 'Smart' interbody cages have added clinical utility compared to sensing spinal implants presented in published studies. As such, future research should aim to improve the implantability of the device by reducing the number of sensors, improving durability, and optimising the sensing configuration.

CRediT authorship contribution statement

Vivek A.S. Ramakrishna: Conceptualization, Methodology, Validation, Formal analysis, Investigation, Data curation, Writing – original draft, Visualisation, Funding acquisition. **Uphar Chamoli:** Conceptualization, Validation, Writing – review & editing, Supervision. **Subhas C. Mukhopadhyay:** Writing – review & editing, Supervision. **Ashish D. Diwan:** Conceptualization, Resources, Writing – review & editing, Supervision. **B. Gangadhara Prusty:** Writing – review & editing, Supervision, Funding acquisition.

Declaration of Competing Interest

The authors declare that they have no known competing financial interests or personal relationships that could have appeared to influence the work reported in this paper.

Acknowledgements

This work was supported by a University of New South Wales Scientia Scholarship awarded to VASR and an AOSpine ANZ grant (AOSAUNZ(R) 2019-03) awarded to BGP and VASR.

Appendix A. Supplementary material

Supplementary data to this article can be found online at https://doi.org/10.1016/j.jbiomech.2023.111440.

References

Borchani, W., Aono, K., Lajnef, N., Chakrabartty, S., 2016. Monitoring of postoperative bone healing using smart trauma-fixation device with integrated self-powered piezo-floating-gate sensors. IEEE Trans. Biomed. Eng. 63, 1463–1472.
Carpenter, C.T., Dietz, J.W., Leung, K.Y., Hanscom, D.A., Wagner, T.A., 1996. Repair of a pseudarthrosis of the lumbar spine. A functional outcome study. J. Bone Joint Surg. Am. 78, 712–720.
Carreon, L.Y., Glassman, S.D., Djurasovic, M., 2007. Reliability and agreement between fine-cut CT scans and plain radiography in the evaluation of posterolateral fusions. Spine J. 7, 39–43.
Carreon, L.Y., Glassman, S.D., Schwender, J.D., Subach, B.R., Gornet, M.F., Ohno, S., 2008. Reliability and accuracy of fine-cut computed tomography scans to determine the status of anterior interbody fusions with metallic cages. Spine J. 8, 998–1002.
Chun, D.S., Baker, K.C., Hsu, W.K., 2015. Lumbar pseudarthrosis: a review of current diagnosis and treatment. Neurosurg. Focus 39, E10.
Demetropoulos, C.K., Morgan, C.R., Sengupta, D.K., Herkowitz, H.N., 2009. Development of a 4-axis load cell used for lumbar interbody load measurements. Med. Eng. Phys. 31, 846–851.
Emami, A., Faloon, M., Sahai, N., Dunn, C.J., Issa, K., Thibaudeau, D., Sinha, K., Hwang, K.S., 2018. Risk factors for pseudarthrosis in minimally-invasive transforaminal lumbar interbody fusion. Asian Spine J. 12, 830–838.
Fogel, G.R., Toohey, J.S., Neidre, A., Brantigan, J.W., 2008. Fusion assessment of posterior lumbar interbody fusion using radiolucent cages: X-ray films and helical

computed tomography scans compared with surgical exploration of fusion. Spine J. 8, 570–577.
Hadley, M.N., Reddy, S.V., 1997. Smoking and the human vertebral column: a review of the impact of cigarette use on vertebral bone metabolism and spinal fusion. Neurosurgery 41, 116–124.
Hayeri, M.R., Tehranzadeh, J., 2009. Diagnostic imaging of spinal fusion and complications. Appl. Radiol. 14–28.
Hopcroft, M.A., Nix, W.D., Kenny, T.W., 2010. What is the Young's Modulus of Silicon? J. Microelectromech. Syst. 19, 229–238.
Hsu, W.K., Nickoli, M.S., Wang, J.C., Lieberman, J.R., An, H.S., Yoon, S.T., Youssef, J.A., Brodke, D.S., McCullough, C.M., 2012. Improving the clinical evidence of bone graft substitute technology in lumbar spine surgery. Global Spine J. 2, 239–248.
Klineberg, E., Gupta, M., McCarthy, I., Hostin, R., 2016. Detection of pseudarthrosis in adult spinal deformity: the use of health-related quality-of-life outcomes to predict pseudarthrosis. Clin. Spine Surg. 29, 318–322.
Ledet, E.H., Tymeson, M.P., DiRisio, D.J., Cohen, B., Uhl, R.L., 2005. Direct real-time measurement of in vivo forces in the lumbar spine. Spine J. 5, 85–94.
Ledet, E.H., D'Lima, D., Westerhoff, P., Szivek, J.A., Wachs, R.A., Bergmann, G., 2012. Implantable sensor technology: from research to clinical practice. J. Am. Acad. Orthop. Surg. 20, 383–392.
Ledet, E.H., Sachs, B.L., Brunski, J.B., Gatto, C.E., Donzelli, P.S., 2000. Real-time in vivo loading in the lumbar spine: part 1. Interbody implant: load cell design and preliminary results. Spine (Phila Pa 1976) 25, 2595–2600.
Lin, J., Walsh, K.W., Jackson, D., Aebersold, J., Crain, M., Naber, J.F., Hnat, W.P., 2007. Davelopment of capacitive pure bending strain sensor for wireless spinal fusion monitoring. Sens. Actuat., A 138, 276–287.
Manzur, M., Virk, S.S., Jivanelli, B., Vaishnav, A.S., McAnany, S.J., Albert, T.J., Iyer, S., Gang, C.H., Qureshi, S., 2019. The rate of fusion for stand-alone anterior lumbar interbody fusion: a systematic review. Spine J. 19, 1294–1301.
Meng, B., Bunch, J., Burton, D., Wang, J., 2021. Lumbar interbody fusion: recent advances in surgical techniques and bone healing strategies. Eur. Spine J. 30, 22–33.
Nakashima, H., Yukawa, Y., Ito, K., Horie, Y., Machino, M., Kanbara, S., Morita, D., Imagama, S., Ishiguro, N., Kato, F., 2011. Extension CT scan: its suitability for assessing fusion after posterior lumbar interbody fusion. Eur. Spine J. 20, 1496–1502.
Orr, J.F., Dunne, N.J., Quinn, J.C., 2003. Shrinkage stresses in bone cement. Biomaterials 24, 2933–2940.
Oshina, M., Oshima, Y., Tanaka, S., Riew, K.D., 2018. Radiological Fusion Criteria of Postoperative Anterior Cervical Discectomy and Fusion: A Systematic Review. Global Spine J. 8, 739–750.
Ramakrishna, V.A.S., Chamoli, U., Rajan, G., Mukhopadhyay, S.C., Prusty, B.G., Diwan, A.D., 2020. Smart orthopaedic implants: A targeted approach for continuous postoperative evaluation in the spine. J. Biomech. 104, 109690.
Ramakrishna, V.A.S., Chamoli, U., Larosa, A.G., Mukhopadhyay, S.C., Prusty, B.G., Diwan, A.D., 2022. Finite element modeling of temporal bone graft changes in XLIF: Quantifying biomechanical effects at adjacent levels. J. Orthop. Res. 40, 1420–1435.
Rohlmann, A., Bergmann, G., Graichen, F., 1994. A spinal fixation device for in vivo load measurement. J. Biomech. 27, 961–967.
Rohlmann, A., Bergmann, G., Graichen, F., 1999. Loads on internal spinal fixators measured in different body positions. Eur Spine J 8, 354–359.
Rohlmann, A., Bergmann, G., Graichen, F., Mayer, H.M., 1995. Telemeterized load measurement using instrumented spinal internal fixators in a patient with degenerative instability. Spine (Phila Pa 1976) 20, 2683–2689.
Sawin, P.D., Dickman, C.A., Crawford, N.R., Melton, M.S., Bichard, W.D., Sonntag, V.K., 2001. The effects of dexamethasone on bone fusion in an experimental model of posterolateral lumbar spinal arthrodesis. J Neurosurg 94, 76–81.
Szivek, J.A., Roberto, R.F., Margolis, D.S., 2005. In vivo strain measurements from hardware and lamina during spine fusion. J Biomed Mater Res B Appl Biomater 75, 243–250.
Umali, J., Ghahreman, A., Diwan, A., 2019. Spinal Fusion Evaluation in Various Settings: A Summary of Human-Only Studies. In: Cheng, B. (Ed.), Handbook of Spine Technology. Springer International Publishing, Cham, pp. 1–17.
Vaidya, R., Sethi, A., Bartol, S., Jacobson, M., Coe, C., Craig, J.G., 2008. Complications in the use of rhBMP-2 in PEEK cages for interbody spinal fusions. J Spinal Disord Tech 21, 557–562.
Wang, Y., Low, K.H., Pang, H.L.J., Hoon, K.H., Che, F.X., Yong, Y.S., 2006. Modeling and simulation for a drop-impact analysis of multi-layered printed circuit boards. Microelectron. Reliab. 46, 558–573.
Windolf, M., Heumann, M., Varjas, V., Constant, C., Ernst, M., Richards, R.G., Wilke, H. J., Benneker, L.M., 2022. Continuous Rod Load Monitoring to Assess Spinal Fusion Status-Pilot In Vivo Data in Sheep. Medicina (Kaunas) 58, 899.
Wu, Z.X., Gong, F.T., Liu, L., Ma, Z.S., Zhang, Y., Zhao, X., Yang, M., Lei, W., Sang, H.X., 2012. A comparative study on screw loosening in osteoporotic lumbar spine fusion between expandable and conventional pedicle screws. Arch. Orthop. Trauma Surg. 132, 471–476.